npj | climate and atmospheric science

Article

Published in partnership with CECCR at King Abdulaziz University

https://doi.org/10.1038/s41612-024-00890-0

Unusual and persistent easterlies restrained the 2023/24 El Niño development after a triple-dip La Niña

Check for updates

Ji-Won Kim[1] ✉, Baijun Tian[1] & Jin-Yi Yu[2] ✉

The 2023/24 El Niño, emerging after a rare triple-dip La Niña, garnered global attention due to its potential to evolve into an extreme event, given the largest accumulation of warm water in the equatorial western Pacific since 1980. Despite initial expectations, its growth rate unexpectedly decelerated in mid-2023, preventing it from reaching the anticipated intensity. Here, we show through observational analyses that unusual easterly anomalies over the tropical western-central Pacific, persisting after the end of the preceding La Niña, significantly contributed to this slowdown. A prominent east–west sea surface temperature gradient in the region has been identified as the crucial factor associated with these unusual and persistent easterly anomalies. This temperature gradient is directly attributed to a negative North Pacific Meridional Mode and a deepened thermocline over the Philippine Sea. These findings offer a deeper understanding of the atypical transition from a prolonged multi-year La Niña to an El Niño.

The onset of the latest El Niño event, commencing in the boreal spring of 2023 (referred to as the 2023/24 El Niño), drew considerable attention due to its emergence following an exceptionally rare triple-dip La Niña event that occurred from 2020 to 2023 and the enhanced risk of causing record-breaking surface temperatures on global or regional scales[1–7]. The accumulation of oceanic heat along the equatorial Pacific during the long-lasting La Niña, conveyed by equatorward Sverdrup transport and considered a major source of El Niño-Southern Oscillation (ENSO) predictability[8–10], was expected to pave the way for a robust El Niño event[2]. By the start of 2023, the warm water volume (WWV), which gauges ocean heat content by integrating water volume above the 20 °C isotherm[10], reached its second-highest value in the entire equatorial Pacific (2.705×10^{15} m^3, as per the WWV index; Supplementary Fig. 1a) and the highest value in the equatorial western Pacific (1.918×10^{15} m^3, as per the WWV_{West} index; Supplementary Fig. 1b) since 1980.

The unprecedented high levels of ocean heat content across the equatorial Pacific prompted global climate centers and bureaus, such as the Climate Prediction Center (CPC) in the United States (https://www.cpc.ncep.noaa.gov/products/precip/CWlink/MJO/enso.shtml) and the Bureau of Meteorology (BOM) in Australia (http://www.bom.gov.au/climate/enso/outlook/), to issue repeated alerts about the upcoming El Niño and predictions of its potential escalation into an extreme event. This event was anticipated to echo the historically devastating extreme El Niño events of 1997–1998 (referred to as the 1997/98 El Niño) and 2015–2016 (referred to as the 2015/16 El Niño)[11–14]. However, the growth rate of the 2023/24 El Niño unexpectedly slowed down after the first half of 2023, falling short of extreme levels. Its Niño3.4 index reached the 2 °C threshold, a common indicator of extreme El Niño events, only once in December 2023 (Supplementary Fig. 2). Consequently, the 2023/24 El Niño event could not be categorized as extreme or very strong[15]. Instead, it was ranked the sixth-strongest El Niño since 1950, following El Niño events in 2015/16 (ranked 1st), 1997/98 (ranked 2nd), 1982/83 (ranked 3rd), 1972/73 (ranked 4th), and 1965/66 (ranked 5th) (https://origin.cpc.ncep.noaa.gov/products/analysis_monitoring/ensostuff/ONI_v5.php). Note that rankings may vary slightly depending on factors such as the region of maximum warming, peak month, choice of datasets and their associated uncertainties, and low-frequency impacts[16,17].

In this study, by analyzing observational data spanning from 1980 to 2023, we revealed the significant role played by unusual and persistent easterly anomalies (departures from average) over the tropical western-central Pacific in explaining why the 2023/24 El Niño, despite experiencing one of the largest oceanic heat accumulations, did not evolve into an extreme event. A notable east-west zonal sea surface temperature (SST) gradient across the region has been identified as a key driver of these easterly anomalies. Additionally, we established a close link between this SST gradient and air-sea coupled variability in the subtropical North Pacific, as well

[1]Jet Propulsion Laboratory, California Institute of Technology, Pasadena, CA, USA. [2]Department of Earth System Science, University of California, Irvine, CA, USA. ✉e-mail: submdus@gmail.com; jyyu@uci.edu

as mean thermocline changes over the Philippine Sea in the tropical western Pacific. These findings not only offer insights into the puzzle surrounding the weaker-than-expected amplitude of the 2023/24 El Niño but also advance our understanding of the atypical transition from multi-year La Niña to El Niño within the ENSO cycle.

Results

Unusual and persistent easterly anomalies

We identified a total of 14 El Niño events occurring between 1980 and 2023, including the 2023/24 El Niño (see "Identifying El Niño events" in Methods; Supplementary Fig. 2). Our analysis primarily focused on comparing the 2023/24 El Niño with the previous extreme El Niño events of 1997/98 and 2015/16. The physical processes underlying these two extreme events, including their triggering and development mechanisms, have been extensively documented in the literature[12,13,18,19]. Therefore, this comparative approach allows us to pinpoint the key processes that prevented the 2023/24 El Niño from evolving into an extreme event such as the 1997/98 and 2015/16 El Niño events. For the remaining 11 El Niño events, we grouped them into the "Other-El Niño" category to further explore whether similar deviations from the two extreme events can be observed or if they are unique to the 2023/24 El Niño. Various climate indices, namely the WWV, U_{WCP}, Niño3.4, ΔSST (comprising the SST_{CP} and SST_{WP}), NPMM, and $D20_{WP}$, were utilized to facilitate comparisons (see "Definition of climate indices" in Methods).

The longitude-time plot of thermocline depth anomalies, represented by the depth of the 20 °C isotherm (D20), clearly shows the accumulation of significant oceanic heat (indicated by positive D20 anomalies) in the equatorial Pacific prior to the onset of the 2023/24 El Niño (Fig. 1a). From 2020 to 2023, this heat accumulation was predominantly concentrated in the western Pacific, with its maximum centered mostly at approximately 120°E in the far-western Pacific (see black stars). The substantial heat accumulation preceding the 2023/24 El Niño resulted from equatorward Sverdrup transport induced by basin-scale easterly anomalies over the tropical Pacific (Fig. 1b), accompanied with the triple-dip La Niña during 2020–2023 (Fig. 1c)[1,2]. The temporal evolution of the WWV index, which integrates warm water volume anomalies across the entire equatorial Pacific, further verifies the accumulated heat conditions before the development of the 2023/24 El Niño (Fig. 1d, red curve). The index shows robust positive WWV values from the preceding year (Year −1) through the boreal spring of the developing year (Year 0) (i.e., February^0 to April^0; delineated by black diagonal lines). During this period, the positive WWV values of the 2023/24 El Niño exceeded those of the two extreme El Niño events (blue and orange curves) and the Other-El Niño group (black curve with gray shading) for most of the time. One prominent exception occurs during the onset spring and summer, when the 1997/98 El Niño exhibits slightly higher WWV values than the 2023/24 El Niño. Hereinafter, the early spring period from February^0 to April^0 will be referred to as "onset spring", during which ENSO events typically initiate, marking their onset stage[20]. Seasons will adhere to Northern Hemisphere conventions.

However, unlike comparable oceanic heat conditions, a stark contrast existed in the atmospheric conditions between the 2023/24 El Niño and the two previous extreme El Niño events. As shown in Fig. 1b, c, the basin-scale

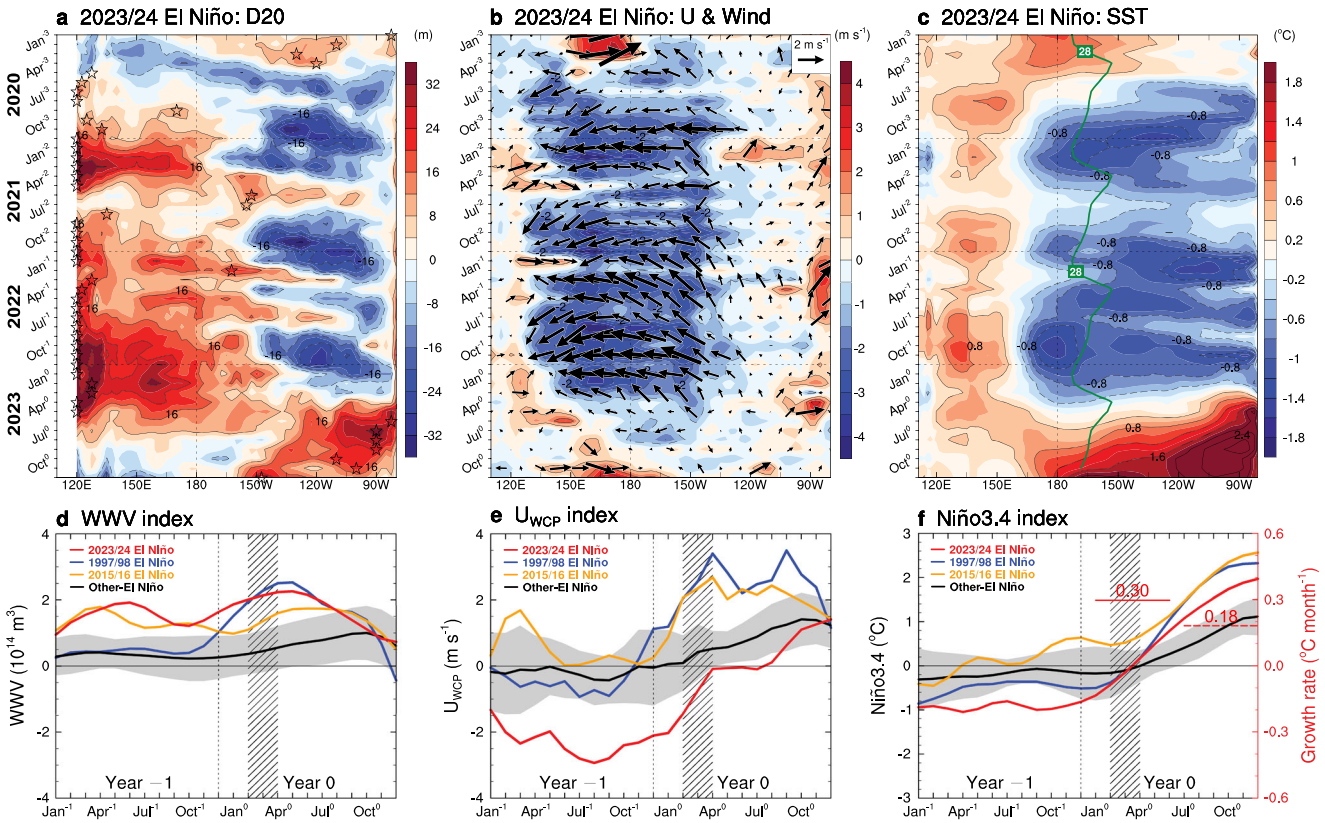

Fig. 1 | Oceanic and atmospheric conditions in the preceding and developing years of the 2023/24 El Niño. Longitude-time plots of anomalous thermocline depth (D20) (**a**), surface zonal wind (U) with horizontal wind vectors (**b**), and sea surface temperature (SST) (**c**) over the tropical Pacific (5°S–5°N) from 2020 to 2023, covering the development of the 2023/24 El Niño. The black contours are overlaid on the shading, with negative values shown as dashed lines. The black stars in (**a**) show the locations of the maximum D20 anomalies. The green contour in **c** marks the climatological 28 °C isotherm line at the equator, which depicts the eastern edge of the western Pacific warm pool. Temporal evolutions of the WWV (**d**), U_{WCP} (**e**), and Niño3.4 (**f**) indices from the preceding (Year −1) to the developing (Year 0) year for the 2023/24, 1997/98, and 2015/16 El Niño events and the Other-El Niño group (gray shading represents ±1 s.d.). The onset spring, from February^0 to April^0, is delineated by black diagonal lines. The red solid and dashed horizontal lines in **f** indicate the growth rate of the Niño3.4 values for the 2023/24 El Niño during the first half, from January^0 to June^0, and the second half, from July^0 to December^0, of the developing year, respectively.

easterly anomalies during the triple-dip La Niña did not dissipate after the demise of the La Niña event. Instead, they persisted into the onset spring of the 2023/24 El Niño. The evolution of the U_{WCP} index (Fig. 1e) confirms the presence of persistent easterly anomalies during the 2023/24 El Niño, with strong negative U_{WCP} values in the preceding year (U_{WCP} index ≤ -2 m s^{-1}), gradually weakening but enduring until April^{0} of the developing year. In contrast, for the two extreme El Niño events, the near-neutral or anomalous easterly wind conditions in the preceding year rapidly transitioned to strong westerly anomalies in the developing year, with U_{WCP} values exceeding 2 m s^{-1} from the onset spring onward. The presence of these strong westerly anomalies, often but not always associated with intraseasonal Madden–Julian Oscillation activity[21], is known to be a key ingredient for triggering extreme El Niño events[22–24]. These wind anomalies carry warm waters from the western Pacific warm pool to the east along the equatorial waveguide by generating a series of downwelling oceanic Kelvin waves, thereby initiating thermocline deepening and surface warming in the tropical eastern Pacific (Supplementary Fig. 3). Meanwhile, the Other-El Niño group of events, on average, experienced nearly neutral atmospheric conditions during the preceding year and then transitioned to weak westerly anomalies in the developing year, with U_{WCP} values close to 0.5 m s^{-1} during the onset spring. Therefore, the stark contrast in onset-spring wind conditions between the 2023/24 El Niño and the 1997/98 and 2015/16 extreme El Niño events is a particularly distinctive feature of the 2023/24 El Niño.

The horizontal maps of surface wind anomalies (Fig. 2a–c) provide further evidence of contrasting atmospheric conditions. During the onset spring, the 2023/24 El Niño was characterized by persistent easterly anomalies over the tropical western-central Pacific (Fig. 2a, black rectangle), whereas the 1997/98 and 2015/16 El Niño events exhibited strong westerly anomalies in the same region (Fig. 2b, c). It is also noticeable that the persistent easterly anomalies during the 2023/24 El Niño confined a larger portion of positive D20 anomalies within the western Pacific (Fig. 2a). This caused the ocean heat content to stagnate in that region until the summer of 2023 (Fig. 1a, b). In contrast, the strong westerly anomalies associated with the two extreme El Niño events allowed the heat content to slosh eastward via eastward-traveling Kelvin waves. These waves transported a larger portion of positive D20 anomalies to the eastern Pacific, leading to the eastward propagation of accumulated heat during the development of the 1997/98 and 2015/16 El Niño events (Fig. 2b, c and Supplementary Fig. 3).

The scatter plot in Fig. 2d displays the onset-spring values of the WWV index against the U_{WCP} index for El Niño events during the analysis period. The plot not only reveals comparable oceanic heat conditions and contrasting atmospheric wind conditions for the 2023/24 El Niño (red dot) compared to the two extreme El Niño events (blue and orange dots), but it also highlights the unusual nature of the 2023/24 El Niño's atmospheric conditions. Specifically, while nearly all El Niño events (11 out of 14; 79%) exhibited anomalous westerly conditions over the tropical western-central Pacific during the onset spring, only three events, including those in 2006/07, 2009/10, and 2023/24, showed the opposite—anomalous easterly conditions. The in-phase relationship between the WWV and U_{WCP} indices among all El Niño events, despite their weak positive correlation ($r = 0.40$, $p = 0.164$), further implies that the anomalous easterly conditions during the onset spring of the 2023/24 El Niño, which coincided with the second-highest WWV value following the 1997/98 El Niño, are historically unusual.

Based on the findings above, we hypothesize that the persistence of unusual easterly anomalies in the tropical western-central Pacific during the spring of 2023 contributes to restraining the 2023/24 El Niño development. Instead of pushing the multi-year-long accumulated heat eastward, these easterly anomalies consistently caused it to stagnate within the western Pacific by piling up warm waters. This heat stagnation hinders the increase of SSTs and the warming/moistening of the overlying air in the tropical central-eastern Pacific, delaying the atmospheric convection needed to establish the Bjerkness feedback[25], which is essential for the growth of an ENSO event. As a result, the 2023/24 El Niño produced weak atmosphere-ocean interactions over the tropical Pacific[26,27], facilitating the prevention of the event's escalation into an extreme El Niño. The temporal evolution of the Niño3.4 index (Fig. 1f) supports this conclusion by revealing a marked deceleration in the Niño3.4 values during the 2023/24 El Niño, after the first half of the developing year. This slowdown is more evident when compared with the two extreme El Niño events. The growth rate of the Niño3.4 values, computed by the slope of a least-squares regression line, decreases by 39% from 0.30 °C month^{-1} during the first half of the developing year to 0.18 °C month^{-1} during the second half (red solid and dashed horizontal lines).

Role of a negative zonal SST gradient

We find that a unique zonal SST gradient across the tropical western-central Pacific during the onset of the 2023/24 El Niño (Fig. 2e) is the main contributor to the unusual and sustained easterly anomalies, contrasting with the pronounced westerly anomalies observed during the onset of two extreme El Niño events. This distinct SST gradient is characterized by a cold anomaly center in the eastern region near the Date Line and a warm anomaly center in the western region over the Philippine Sea (Fig. 2e, black dashed and solid rectangles). In contrast, the two extreme events exhibit an opposite pattern overall, with warm anomalies in the tropical central Pacific and cold anomalies in the western Pacific (Fig. 2f, g). The scatter plot in Fig. 2h demonstrates a robust in-phase relationship between the intensities of the zonal SST gradient across the tropical western-central Pacific (ΔSST index) and the zonal wind anomalies averaged in the region (U_{WCP} index) for El Niño events. A significant positive correlation ($r = 0.81$, $p < 0.01$) indicates that the zonal SST gradient accounts for 66% of the variance in zonal wind. The plot further underscores the striking divergence in the ΔSST indices between the 2023/24 El Niño and the two extreme El Niño events, with the former showing the most pronounced negative gradient and the latter exhibiting the first and fourth strongest positive gradients. Corresponding to these differing zonal SST gradients, the 2023/24 El Niño resulted in the second strongest easterly anomalies, whereas the two extreme El Niño events produced the two strongest westerly anomalies among all events. These results suggest that the negative zonal SST gradient in the tropical western-central Pacific is closely associated with the unusual easterly anomalies observed during the 2023/24 El Niño's onset spring.

The prominent negative zonal SST gradient associated with the 2023/24 El Niño induces analogous diabatic heating anomalies in the tropical western-central Pacific (Fig. 3a, black rectangle), promptly suppressing atmospheric deep convection in the east, as indicated by positive outgoing longwave radiation (OLR) anomalies, while enhancing it in the west, as indicated by negative OLR anomalies. The suppression of atmospheric convection in the tropical central Pacific is more pronounced than the enhanced convection in the tropical western Pacific. This difference is attributed to the cold anomalies present in the tropical central Pacific, which effectively lower SSTs below the convective threshold of ~28 °C[28] (green contours in Figs. 1c and 2e), thereby switching off deep convection and inducing stronger diabatic heating anomalies[29,30]. The changes in atmospheric convection subsequently form a regional zonal overturning circulation (Fig. 3b), with its descending branch near the Date Line and its ascending branch positioned over the Maritime Continent. This circulation is characterized by a clockwise anomalous wind flow, contributing to the generation of easterly anomalies at the surface and their persistence during the onset spring of the 2023/24 El Niño (Fig. 1b, e). The zonal structures of OLR, SST, and zonal wind anomalies averaged within the tropical band (Fig. 3c) further support the aforementioned processes. Conversely, these processes are in general opposite for the two extreme El Niño events (Supplementary Fig. 4): an enhanced/suppressed atmospheric deep convection in the tropical central/western Pacific and a counterclockwise zonal overturning circulation in the tropical western-central Pacific, producing westerly anomalies at the surface during their onset spring.

Tropical central Pacific cooling

What caused the negative zonal SST gradient across the tropical western-central Pacific during the onset stage of the 2023/24 El Niño? To answer this question, we perform a further analysis by breaking it down into two

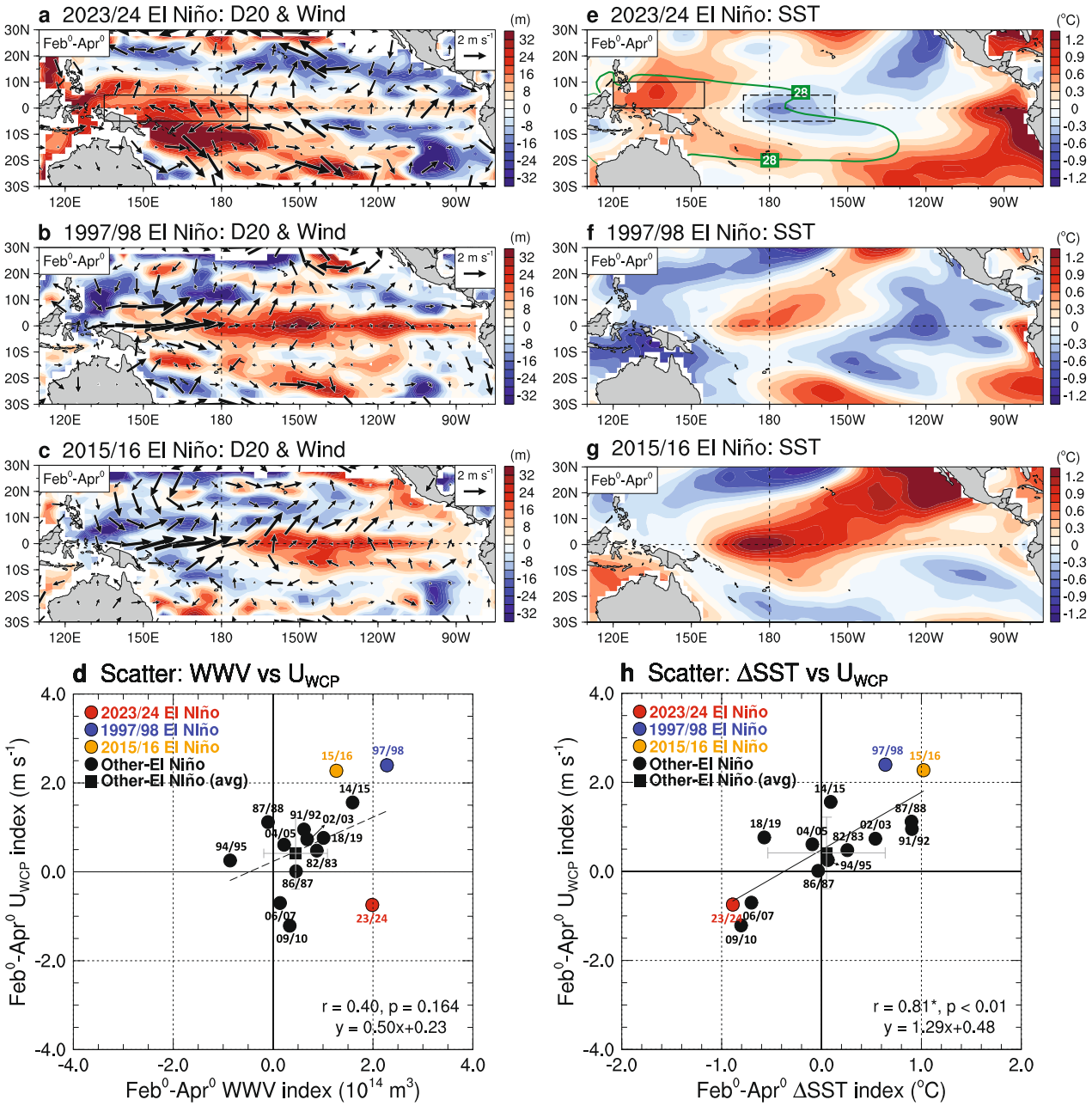

Fig. 2 | Contrasting atmospheric conditions of the 2023/24 El Niño driven by the zonal sea surface temperature gradient. Horizontal maps showing anomalous thermocline depth (D20) and surface wind vectors during February^0 to April^0 (as the onset spring) for the 2023/24 (**a**), 1997/98 (**b**), and 2015/16 (**c**) El Niño events. **d** Scatter plot of the WWV index against U_{WCP} index during the onset spring for the three El Niño events and the Other-El Niño group (error bars indicating ±1 s.d.) Same as (**a**–**c**), except for the anomalous sea surface temperature (SST). The green contour in (**e**) marks the climatological 28 °C isotherm, denoting the western Pacific warm pool and the SST threshold for tropical deep convection. **h** Same as (**d**) but for the ΔSST index on the x-axis. In (**d**) and (**h**), the black lines are obtained through linear regression among all the dots and are expressed as solid (dashed) when their correlation coefficient (*r*) is statistically significant (insignificant).

components: tropical central Pacific cooling and tropical western Pacific warming, as discussed in this and subsequent sections, respectively.

For tropical central Pacific cooling (i.e., the eastern component of the negative zonal SST gradient; black dashed rectangle in Fig. 2e), we identify the subtropical Pacific coupling processes associated with the North Pacific Meridional Mode (NPMM)[31] as playing a pivotal role. Studies have shown that the NPMM can influence tropical Pacific variability and contribute to the increasing complexity of ENSO events in terms of both spatial patterns and temporal evolutions[32–39]. In the winter preceding the 2023/24 El Niño (i.e., November^{-1} to January^0), when the third La Niña of the 2020–2023 triple-dip event evolves into its mature-to-decay stage (Fig. 1c), cold SST anomalies associated with La Niña extend further west, centered in the tropical central Pacific (Fig. 4a). The maximum cold SST anomaly is located near the Date Line, crossing the eastern edge of the western Pacific warm pool, as delineated by the white star and green contour on the map. These cold anomalies in the tropical central Pacific induce strong diabatic heating anomalies by effectively suppressing deep convection[1,30], readily triggering stationary atmospheric Rossby waves into the North Pacific[40] and forming an anomalous anticyclone east of Hawaii in the following spring, including the NPMM region (Fig. 4b, black parallelogram). This subtropical

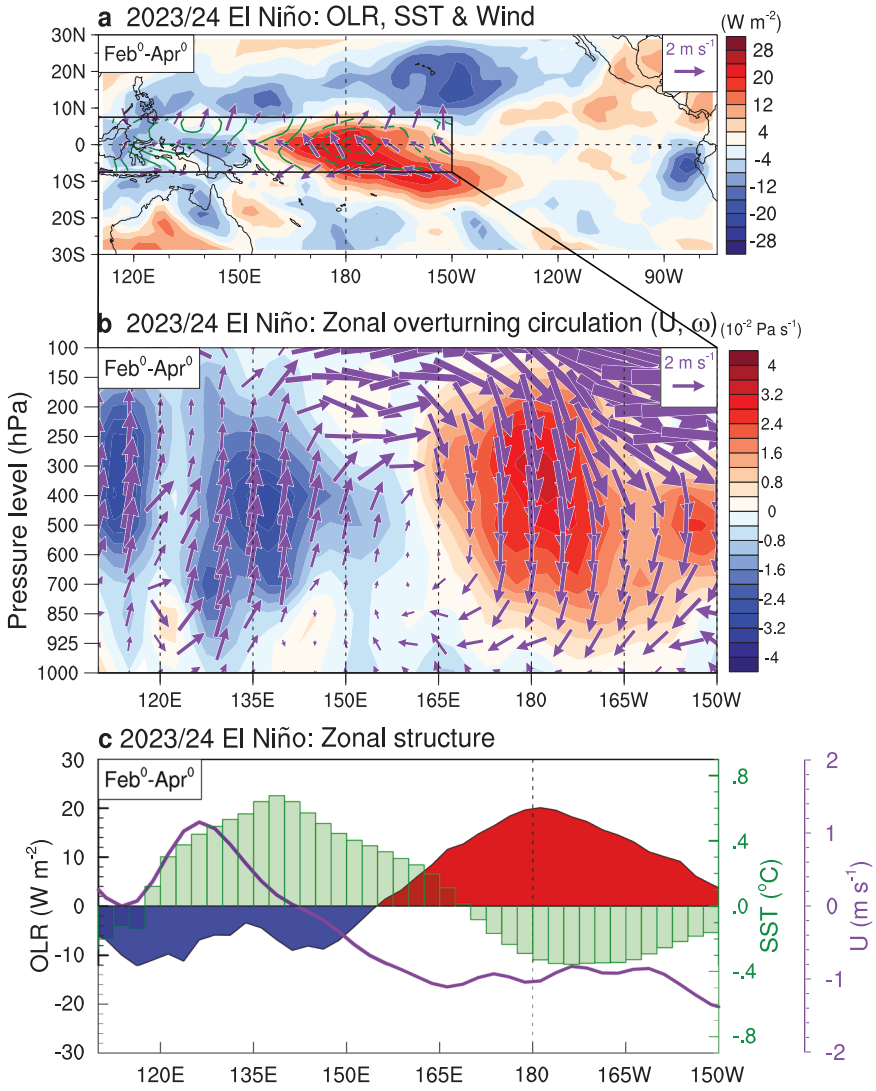

Fig. 3 | Processes behind the generation of unusual and persistent easterly anomalies during the 2023/24 El Niño. a Horizontal map showing anomalous outgoing longwave radiation (OLR; shading), sea surface temperature (SST; green contours, with negative values shown as dashed lines), and surface wind (purple vector) during February^0 to April^0 (as the onset spring) of the 2023/24 El Niño. **b** Zonal overturning circulation (purple vector) and anomalous vertical velocity (ω; shading) across the tropical band from 7.5°S–7.5°N to 110°E–150°W (black rectangular region in **a**) during the onset spring. The circulation is derived from anomalous zonal winds and ω fields (scaled by a factor of 100) on pressure levels. **c** Zonal structure over the tropical band depicting anomalous OLR (shading), SST (green bar-chart), and surface zonal wind (U; purple contour) during the onset spring.

anomalous anticyclone, characterized by clockwise surface wind and positive sea level pressure anomalies, initiates a band of cold anomalies from Baja California toward the equator through the so-called Wind-Evaporation-SST (WES) feedback—a thermodynamic positive feedback loop involving air-sea coupling processes that alter surface winds, evaporation rates, and SSTs[41]. The resulting cold SST anomalies in the subtropical North Pacific, accompanied by northeasterly anomalies, demonstrate the defining characteristics of a negative phase of the NPMM. Thus, we infer that a negative NPMM event, stemming from the preceding La Niña, occurred during the onset of the 2023/24 El Niño. Once a negative NPMM begins, it can be maintained for several months via the WES feedback and/or the trade wind charging mechanism driven by wind stress curl anomalies[42], spreading cold anomalies into the tropical central Pacific and leading to SST cooling in that region (Fig. 4b, black dashed rectangle).

The temporal evolution of the NPMM index (Fig. 4c) and its seasonally averaged intensity during the onset spring (Fig. 4d) provide evidence supporting this conclusion. For the 2023/24 El Niño, the NPMM values decrease rapidly from the preceding winter, turning negative in the onset spring (NPMM index ≈ −1 s.d.) and reaching their minimum in July^0 (Fig. 4c, d, red curve and bar-chart). A recent study proposed that the minimum peak of a negative NPMM during summer is likely triggered by SST anomalies in the Atlantic Ocean, particularly an intense North Atlantic Tripole SST pattern[27]. In contrast, the NPMM values for both the extreme 1997/98 and 2015/16 El Niño events, as well as for the Other-El Niño group, remain positive during their onset spring and afterward, indicating the presence of a positive NPMM (Fig. 4c, d, blue, orange, and black curves and bar-charts). This suggests that the occurrence of a negative NPMM during an El Niño event, as observed in the 2023/24 El Niño, is unique. Note that the positive NPMM event was especially strong for the 2015/16 El Niño, as depicted in Fig. 2g, and hence caused stronger SST warming in the tropical central Pacific compared to the 1997/98 El Niño (Fig. 2f, g and Supplementary Fig. 3c, f). This strong positive NPMM event in the 2015/16 El Niño was understood through interactions within the tropical and subtropical Pacific Oceans linked to a preceding central Pacific-type El Niño in 2014/15[19,34,43,44].

The scatter plot in Fig. 4e illustrates the relationship between the NPMM and SST_{CP} indices during the onset spring of El Niño events. This highlights the uniqueness of the 2023/24 El Niño case, which represents the strongest negative NPMM value among all the events. The plot also supports our claim by revealing a positive correlation between the two indices ($r = 0.46$, $p < 0.1$), indicating an in-phase relationship between the strength of the subtropical NPMM events and the change in the tropical central Pacific SST. The regression map of SST anomalies with respect to the inversed NPMM index (Fig. 4f) further corroborates this, as it shows significant cold anomalies aligned in a northeast-southwest direction from the subtropical North Pacific to the tropical central Pacific.

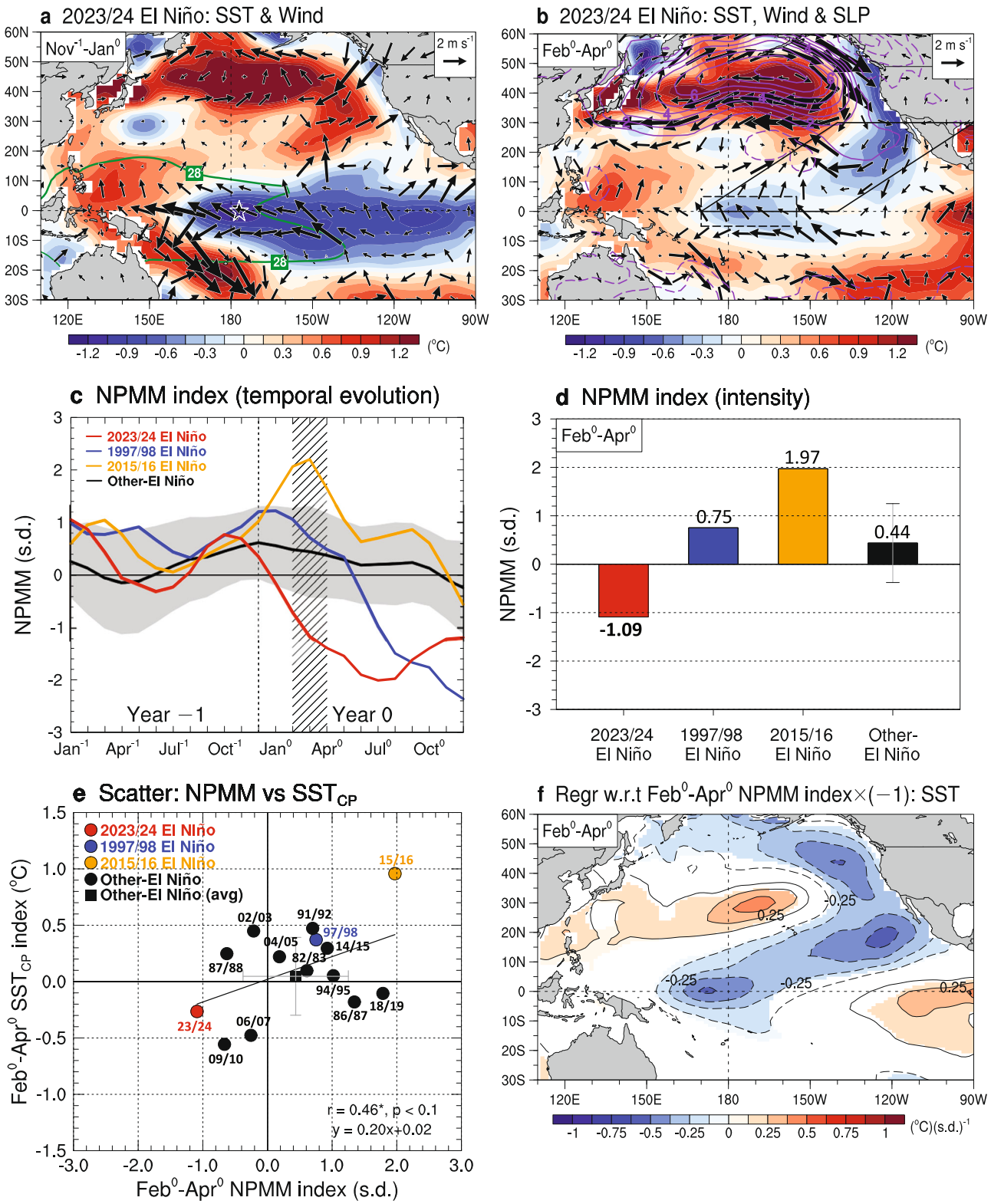

Fig. 4 | Negative North Pacific Meridional Mode (NPMM) linked to tropical central Pacific cooling. a Horizontal map showing the anomalous sea surface temperature (SST; shading) and surface wind (vector) during November^{-1} to January^{0} of the 2023/24 El Niño. The white star and green contour depict the location of the minimum SST anomaly and the climatological 28 °C isotherm, respectively. **b** Same as (**a**) but during February^{0} to April^{0} (as the onset spring), with contours denoting sea level pressure (SLP) anomalies. **c** Temporal evolution of the NPMM index from the preceding to the developing years for the 2023/24, 1997/98, and 2015/16 El Niño events and the Other-El Niño group (gray shading representing ±1 s.d.), with the onset spring delineated by black diagonal lines. **d** Bar-chart of seasonally-averaged NPMM intensity during the onset spring for the three El Niño events and the Other-El Niño group (error bars indicating ±1 s.d.). **e** Scatter plot of the NPMM index against the SST_{CP} index during the onset spring for the three El Niño events and the Other-El Niño group (error bars indicating ±1 s.d.). **f** Regression map of anomalous SST with respect to the inversed NPMM index (multiplied by −1) during the onset spring. Shaded areas indicate regression coefficients that exceed a significance level of 0.1.

Tropical western Pacific warming

Regarding tropical western Pacific warming (i.e., the western component of the negative zonal SST gradient; black solid rectangle in Fig. 2e), we identify a deepened thermocline over the Philippine Sea before the onset of the 2023/24 El Niño as a crucial factor. During the preceding winter of the 2023/24 El Niño (Fig. 5a), the thermocline notably deepened across the entire western Pacific, covering the Philippine Sea region corresponding to tropical western Pacific warming (see black rectangle). As previously demonstrated, this deepening of the thermocline was caused by prolonged basin-scale easterly anomalies associated with the preceding La Niña, which resulted in the largest heat accumulation in the western Pacific (Fig. 1a–c and Supplementary Fig. 1b). Nevertheless, caution is warranted in attributing this local thermocline deepening to the preceding La Niña, as it may result solely from the last event of the triple-dip La Niña rather than from the two earlier events. Further detailed analysis is needed to determine whether a triple-dip La Niña could yield a cumulative effect on thermocline changes in the tropical western Pacific and, if so, to clarify the underlying mechanism.

Our lead-lag correlation analysis (Fig. 5b) shows that the SST anomaly in the tropical western Pacific, averaged from February^{0} to April^{0} (referred to as the SST_{WP} index), is most positively correlated with the in-situ $D20_{WP}$ variation in the preceding December^{-1}, as indicated by the black star. This suggests that SST warming in the tropical western Pacific lags the thermocline deepening by approximately one season. This lag time occurs because, as the thermocline deepens within the subsurface ocean layer (up to ~300 m), the response of the overlying SSTs to thermocline depth variation becomes slower, necessitating additional adjustment time[45,46].

The temporal progression of the $D20_{WP}$ index (Fig. 5c), along with its intensity averaged over the preceding winter (Fig. 5d; delineated by black stippling in Fig. 5c), underscores the distinctiveness of the thermocline deepening associated with the 2023/24 El Niño when compared to all other events. The $D20_{WP}$ values are strongly positive during the 2023/24 El Niño, from the preceding year until the spring of the developing year, almost reaching 2 s.d. in the preceding winter. However, the $D20_{WP}$ values for the two extreme 1997/98 and 2015/16 El Niño events, as well as for the Other-El Niño group, mostly exhibit only weak positive or near-zero values during the same period. The scatter plot in Fig. 5e, illustrating the relationship between the preceding winter $D20_{WP}$ index and the onset spring SST_{WP} index for El Niño events, further supports the aforementioned findings. The $D20_{WP}$ and SST_{WP} indices have the highest values during the 2023/24 El Niño, with a robust in-phase relationship between the two indices ($r = 0.67$, $p < 0.05$). These results collectively suggest that the deepened thermocline over the Philippine Sea in the preceding winter played a critical role in generating tropical western Pacific warming during the onset spring of the 2023/24 El Niño. The lagged regression map of SST anomalies with respect to the preceding winter $D20_{WP}$ index (Fig. 5f) also substantiates our suggestion by disclosing significant warm anomalies in the tropical western Pacific, including the Philippine Sea region.

Discussion

This study provides insights into the unexpected deceleration of El Niño development after the first half of 2023, linking this deceleration to a unique regional atmosphere-ocean coupling that emerged in the tropical western-central Pacific at the event's onset stage. This regional coupling, initiated by a local negative zonal SST gradient, contributed to the formation of unusual and persistent easterly anomalies near the surface over the tropical western-central Pacific. These anomalies, in turn, hindered the eastward propagation of the substantial western Pacific heat content accumulated from the preceding triple-dip La Niña. This hindrance ultimately restrained the 2023/24 El Niño from intensifying into an extreme event akin to those witnessed in 1997/98 and 2015/16, despite comparable levels of ocean heat content across these events. We found that the origin of the negative zonal SST gradient is closely related to the residual oceanic and atmospheric conditions following the decay of the preceding La Niña. These residual conditions played a significant role in triggering a negative NPMM in the subtropical North Pacific and deepening the mean thermocline over the Philippine Sea, which led to the cold and warm anomaly poles of the zonal SST gradient, respectively. Aside from the role of the negative zonal SST gradient identified in this study, it is worth mentioning that the easterly anomalies over the tropical western-central Pacific may also arise from other factors. These include the meridional gradient in cross-equatorial Pacific sea level pressure anomalies[26], interdecadal changes in the mean state that have strengthened the tropical Pacific zonal SST contrast[47], and inter-basin remote impacts from tropical Indian Ocean warming[48].

Finally, this study highlights that the 2023/24 El Niño failed to attain the anticipated extreme strength due to the competition between tropical ENSO dynamics involving the equatorial Pacific ocean heat content and subtropical ENSO dynamics involving the NPMM events. While these two types of ENSO dynamics[46] have been emphasized in explaining different spatial patterns (e.g., eastern Pacific-type vs. central Pacific-type)[43,49,50] and temporal evolutions (e.g., single-year vs. multi-year)[33,34,51] of individual ENSO events, the 2023/24 El Niño presents a novel and significant opportunity to realize that the mutual interference between these two dynamics is crucial for the development of extreme events. For instance, when the two types of ENSO dynamics compete with each other through large equatorial heat accumulation and a negative NPMM, they can prevent an El Niño from developing into an extreme event, as observed in the case of the 2023/24 El Niño. However, these dynamics can also collaborate, as seen in the case of the 2015/16 El Niño with large equatorial heat accumulation and a positive NPMM, to facilitate the occurrence of extreme events.

Methods

Observational data

We analyzed a variety of monthly mean observational datasets covering the period from January 1980 to December 2023. For sea surface temperature (SST), we used the National Oceanic and Atmospheric Administration (NOAA) Extended Reconstructed SST version 5 (ERSSTv5) data[52], which spanned from January 1854 to the present. Atmospheric variables, including zonal and meridional winds (U and V), vertical velocity on pressure levels (ω), and sea level pressure (SLP), were obtained from the National Centers for Environmental Prediction–Department of Energy (NCEP–DOE) Reanalysis 2 data[53] covering the period from January 1979 to the present. The outgoing longwave radiation (OLR) data were provided by the NOAA Climate Data Record (CDR)[54], which spans from January 1979 to the present. Additionally, thermocline depth (D20), defined as the depth of the 20 °C isotherm, was extracted from the NCEP Global Ocean Data Assimilation System (GODAS) data[55], available from January 1980 onward. All anomalies in this study were computed as departures by subtracting the climatological seasonal cycle for the latest 30-year base period of 1991–2020.

Identifying El Niño events

According to the definition provided by the NOAA Climate Prediction Center (CPC), an El Niño event is identified as occurring when a minimum of five consecutive overlapping three-month running means of SST anomalies in the ENSO monitoring region (i.e., the Niño3.4 region between 170°W–120°W, 5°S–5°N) are at or above 0.5 °C. Applying this definition, we identified a total of 14 El Niño events during the observation period spanning from 1980 to 2023. These years include: 1982/83, 1986/87, 1987/88, 1991/92, 1994/95, 1997/98, 2002/03, 2004/05, 2006/07, 2009/10, 2014/15, 2015/16, 2018/19, and 2023/24. Note that the specific years of El Niño events were marked in the scatter plots throughout the manuscript to help identify which El Niño years deviate from expectations based on the relationship between two climate indices.

Definition of climate indices

Various climate indices were utilized in this study. The Niño3.4 index, commonly used for monitoring the oceanic conditions of ENSO, is defined as the SST anomaly averaged in the Niño3.4 region in the tropical Pacific between 170°W–120°W and 5°S–5°N. The warm water volume (WWV) index, originally developed by Meinen and McPhaden[10], is widely used for measuring equatorial Pacific heat content. It is defined as the water volume

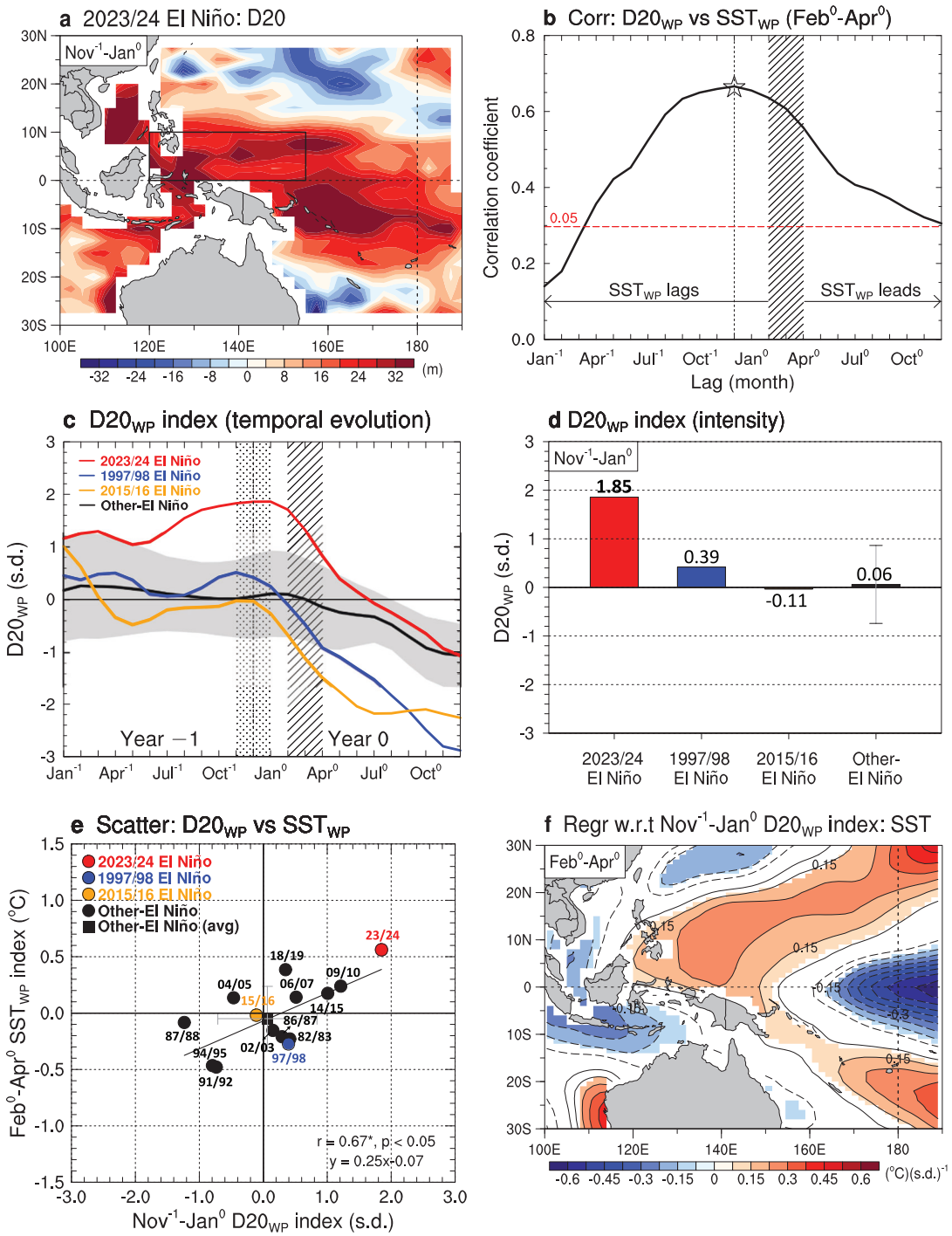

Fig. 5 | Deepened thermocline over the Philippine Sea linked to tropical western Pacific warming. a Horizontal map showing anomalous thermocline depth (D20) during November^{-1} to January^{0} (as the preceding winter) for the 2023/24 El Niño. **b** Lead-lag correlation between the monthly $D20_{WP}$ index and the seasonally-averaged SST_{WP} index during February^{0} to April^{0} (as the onset spring; shaded with black diagonal lines). The black star and red dashed line denote the location of the maximum correlation and the 0.05 significance level, respectively. **c** Temporal evolution of the $D20_{WP}$ index from the preceding to the developing years for the 2023/24, 1997/98, and 2015/16 El Niño events and the Other-El Niño group (gray shading represents ±1 s.d.). The preceding winter and onset spring are delineated by black stippling and diagonal lines, respectively. **d** Bar-chart of seasonally-averaged $D20_{WP}$ intensity during the preceding winter for the three El Niño events and the Other-El Niño group (error bars indicating ±1 s.d.). **e** Scatter plot of the preceding winter $D20_{WP}$ index against the onset spring SST_{WP} index for the three El Niño events and the Other-El Niño group (error bars indicating ±1 s.d.). **f** Regression map of anomalous SST during the onset spring with respect to the preceding winter $D20_{WP}$ index. Shaded areas indicate regression coefficients that exceed a significance level of 0.1.

(raw or anomaly) integrated above the 20 °C isotherm in the entire Pacific region between 120°E–80°W and 5°S–5°N. The WWV_{West} index is defined similarly to the WWV index, except that it pertains to the western Pacific region between 120°E–155°W and 5°S–5°N. The U_{WCP} index quantifies the strength of zonal wind near the surface. It is defined as the surface zonal wind anomaly averaged in the tropical western-central Pacific region between 135°E–170°W and 5°S–5°N. The ΔSST index quantifies the strength of the zonal SST gradient in the tropical western-central Pacific. It is defined as the area-average difference of SST anomalies between the tropical central Pacific (170°E–155°W, 5°S–5°N; as in the SST_{CP} index) and the western Pacific (120°E–155°E, 0–10°N; as in the SST_{WP} index). The North Pacific Meridional Mode (NPMM) index was originally introduced by Chiang and Vimont[31] and represents the coupled variability of SST and wind patterns over the subtropical North Pacific. It is defined as the normalized SST expansion coefficient (in the first mode) obtained from the singular value decomposition (SVD) analysis[56]. This SVD analysis is conducted on the cross-covariance matrix between anomalous SST and 10 m wind data within the region spanning from 21°S–32°N and 175°E–95°W, with ENSO signals removed via linear regression with respect to the cold tongue index (i.e., SST anomaly averaged over 180°E–90°W and 6°S–6°N). The $D20_{WP}$ index quantifies the change in the mean thermocline depth in the tropical western Pacific. It is defined as the normalized D20 anomaly averaged in the tropical western Pacific between 120°E–155°E and 0–10°N. The climate indices prior to the analysis were smoothed using a 3-month running-mean filter to reduce the effects of intraseasonal variability.

Statistical significance test

The standard deviation (s.d.) was calculated to assess the statistical robustness of the observed changes in the climate indices utilized in this study. A *t*-statistic was computed to evaluate the statistical significance of the estimated coefficients from correlation and regression analyses. The formula for the *t*-statistic is as follows:

$$t = \frac{estimated\ coefficient}{standard\ error} \quad (1)$$

The standard error quantifies the variability in the estimated coefficient that would arise from taking multiple samples from the same population. Next, we computed a *p*-value for the *t*-statistic, which represents the probability of observing a *t*-statistic as extreme as the computed one under the null hypothesis, i.e., H_0 = the variable does not have a significant effect on the dependent variable. In the analysis, if the *p*-value is less than the significance level of 0.1 (corresponding to the 90% confidence level), we reject the null hypothesis and conclude that the coefficient is statistically significant.

Data availability

The data related to the paper are publicly available and can be downloaded from the following websites: ERSSTv5, https://psl.noaa.gov/data/gridded/data.noaa.ersst.v5.html; NCEP-DOE Reanalysis 2, https://psl.noaa.gov/data/gridded/data.ncep.reanalysis2.html; NOAA CDR, https://www.ncei.noaa.gov/data/outgoing-longwave-radiation-monthly/access/; GODAS, https://psl.noaa.gov/data/gridded/data.godas.html; WWV index, https://www.pmel.noaa.gov/elNiño/upper-ocean-heat-content-and-enso; NPMM index, https://www.aos.wisc.edu/dvimont/MModes/PMM.html.

Code availability

All codes used for the analysis are available upon request from the corresponding author, J.-W.K. The codes were developed using the NCAR Command Language (NCL; https://www.ncl.ucar.edu/), which is a public access software.

Received: 26 September 2024; Accepted: 23 December 2024;
Published online: 27 January 2025

References

1. Kim, J. W., Yu, J. Y. & Tian, B. Overemphasized role of preceding strong El Niño in generating multi-year La Niña events. *Nat. Commun.* **14**, 6790 (2023).
2. Lian, T., Wang, J., Chen, D., Liu, T. & Wang, D. A strong 2023/24 El Niño is staged by tropical Pacific Ocean heat content buildup. *Ocean-Land-Atmos. Res.* **2**, 0011 (2023).
3. Li, K., Zheng, F., Cheng, L., Zhang, T. & Zhu, J. Record-breaking global temperature and crises with strong El Niño in 2023–2024. *Innov. Geosci.* **1**, 100030 (2023).
4. Li, X., Hu, Z. Z., Tseng, Y. H., Liu, Y. & Liang, P. A historical perspective of the La Niña event in 2020/2021. *J. Geophys. Res. Atmos.* **127**, e2021JD035546 (2022).
5. Fang, X., et al. Will the historic southeasterly wind over the equatorial Pacific in March 2022 trigger a third-year La Niña event? *Adv. Atmos. Sci.* (2023).
6. McPhaden, M. J. The 2020–22 triple-dip La Niña [in "State of the Climate in 2022"]. *Bull. Am. Meteorol. Soc.* **104**, S157–S158 (2023).
7. Jiang, N. et al. Enhanced risk of record-breaking regional temperatures during the 2023–24 El Niño. *Sci. Rep.* **14**, 2521 (2024).
8. Wyrtki, K. Water displacements in the Pacific and the genesis of El Niño cycles. *J. Geophys. Res. Oceans* **90**, 7129–7132 (1985).
9. Jin, F. F. An equatorial ocean recharge paradigm for ENSO. Part I: conceptual model. *J. Atmos. Sci.* **54**, 811–829 (1997).
10. Meinen, C. S. & McPhaden, M. J. Observations of warm water volume changes in the equatorial Pacific and their relationship to El Niño and La Niña. *J. Clim.* **13**, 3551–3559 (2000).
11. Bayer, A. M. et al. An unforgettable event: a qualitative study of the 1997–98 El Niño in northern Peru. *Disasters* **38**, 351–374 (2014).
12. Paek, H., Yu, J. Y. & Qian, C. Why were the 2015/2016 and 1997/1998 extreme El Niños different? *Geophys. Res. Lett.* **44**, 1848–1856 (2017).
13. Santoso, A., Mcphaden, M. J. & Cai, W. The defining characteristics of ENSO extremes and the strong 2015/2016 El Niño. *Rev. Geophys.* **55**, 1079–1129 (2017).
14. Newman, M., Wittenberg, A. T., Cheng, L., Compo, G. P. & Smith, C. A. The extreme 2015/16 El Niño, in the context of historical climate variability and change. *Bull. Am. Meteor. Soc.* **99**, S16–S20 (2018).
15. Trenberth, K. & National Center for Atmospheric Research Staff (Eds). Last modified 2024-03-20 "The Climate Data Guide: Niño SST Indices (Niño 1+2, 3, 3.4, 4; ONI and TNI)".
16. Huang, B., L'Heureux, M., Hu, Z. Z. & Zhang, H. M. Ranking the strongest ENSO events while incorporating SST uncertainty. *Geophys. Res. Lett.* **43**, 9165–9172 (2016).
17. Li, X., Hu, Z. Z. & Huang, B. Contributions of atmosphere–ocean interaction and low-frequency variation to intensity of strong El Niño events since 1979. *J. Clim.* **32**, 1381–1394 (2019).
18. Lengaigne, M. et al. The March 1997 westerly wind event and the onset of the 1997/98 El Niño: understanding the role of the atmospheric response. *J. Clim.* **16**, 3330–3343 (2003).
19. Kim, J. W. & Yu, J. Y. Understanding reintensified multiyear El Niño events. *Geophys. Res. Lett.* **47**, e2020GL087644 (2020).
20. Park, J. H. et al. Mid-latitude leading double-dip La Niña. *Int. J. Climatol.* **41**, E1353–E1370 (2021).
21. McPhaden, M. J. & Yu, X. Equatorial waves and the 1997–98 El Niño. *Geophys. Res. Lett.* **26**, 2961–2964 (1999).
22. Kessler, W. S. Is ENSO a cycle or a series of events? *Geophys. Res. Lett.* **29**, 40–41 (2002).
23. Fedorov, A. V., Hu, S., Lengaigne, M. & Guilyardi, E. The impact of westerly wind bursts and ocean initial state on the development, and diversity of El Niño events. *Clim. Dyn.* **44**, 1381–1401 (2015).
24. Kim, J. W. & An, S. I. Origin of early-spring central Pacific warming as the 1982–1983 El Niño precursor. *Int. J. Climatol.* **38**, 2899–2906 (2018).
25. Bjerknes, J. Atmospheric teleconnections from the equatorial Pacific. *Monthly Weather Rev.* **97**, 163–172 (1969).

26. Tan, W. et al. On the divergent evolution of ENSO after the coastal El Niños in 2017 and 2023. *Geophys. Res. Lett.* **51**, e2024GL108198 (2024).
27. Hong, C. C., Sullivan, A. & Chang, C. C. Impact of North Atlantic tripole and extratropical North Pacific extreme SSTs on the 2023/24 El Niño. *Geophys. Res. Lett.* **51**, e2024GL110639 (2024).
28. Sud, Y. C., Walker, G. K. & Lau, K. M. Mechanisms regulating sea-surface temperatures and deep convection in the tropics. *Geophys. Res. Lett.* **26**, 1019–1022 (1999).
29. Hoerling, M. P., Kumar, A. & Zhong, M. El Niño, La Niña, and the nonlinearity of their teleconnections. *J. Clim.* **10**, 1769–1786 (1997).
30. Fang, S. W. & Yu, J. Y. A control of ENSO transition complexity by tropical Pacific mean SSTs through tropical-subtropical interaction. *Geophys. Res. Lett.* **47**, e2020GL087933 (2020).
31. Chiang, J. C. & Vimont, D. J. Analogous Pacific and Atlantic meridional modes of tropical atmosphere–ocean variability. *J. Clim.* **17**, 4143–4158 (2004).
32. Capotondi, A. et al. Understanding ENSO diversity. *Bull. Am. Meteorol. Soc.* **96**, 921–938 (2015).
33. Yu, J. Y. & Fang, S. W. The distinct contributions of the seasonal footprinting and charged-discharged mechanisms to ENSO complexity. *Geophys. Res. Lett.* **45**, 6611–6618 (2018).
34. Kim, J. W. & Yu, J. Y. Single-and multi-year ENSO events controlled by pantropical climate interactions. *npj Clim. Atmos. Sci.* **5**, 88 (2022).
35. Kim, J. W. & Yu, J. Y. Evolution of subtropical Pacific-onset El Niño: how its onset location controls its decay evolution. *Geophys. Res. Lett.* **48**, e2020GL091345 (2021).
36. Chen, J. et al. Tropical and subtropical Pacific sources of the asymmetric El Niño-La Niña decay and their future changes. *Geophys. Res. Lett.* **49**, e2022GL097751 (2022).
37. Fan, H., Wang, C. & Yang, S. Asymmetry between positive and negative phases of the Pacific meridional mode: a contributor to ENSO transition complexity. *Geophys. Res. Lett.* **50**, e2023GL104000 (2023).
38. Kim, J. W., Chang, T. H., Lee, C. T. & Yu, J. Y. Evaluating ENSO's spatiotemporal complexity in the CWB CFS 1-tiered model hindcasts. *J. Geophys. Res.: Atmos.* **128**, e2022JD038200 (2023).
39. Li, X., Yu, J. Y. & Ding, R. El Niño-La Niña asymmetries in the changes of ENSO complexities and dynamics since 1990. *Geophys. Res. Lett.* **51**, e2023GL106395 (2024).
40. Hoskins, B. J. & Karoly, D. J. The steady linear response of a spherical atmosphere to thermal and orographic forcing. *J. Atmos. Sci.* **38**, 1179–1196 (1981).
41. Xie, S. P. & Philander, S. G. H. A coupled ocean-atmosphere model of relevance to the ITCZ in the eastern Pacific. *Tellus A* **46**, 340–350 (1994).
42. Anderson, B. T. & Perez, R. C. ENSO and non-ENSO induced charging and discharging of the equatorial Pacific. *Clim. Dyn.* **45**, 2309–2327 (2015).
43. Kao, H. Y. & Yu, J. Y. Contrasting eastern-Pacific and central-Pacific types of ENSO. *J. Clim.* **22**, 615–632 (2009).
44. Ding, R. et al. Multi-year El Niño events tied to the North Pacific oscillation. *Nat. Commun.* **13**, 3871 (2022).
45. An, S. I., Tziperman, E., Okumura, Y. M., & Li, T. ENSO irregularity and asymmetry. *El Niño Southern Oscillation in a Changing Climate*, 153–172 (Wiley, 2020).
46. Yu, J. Y., Wang, X., Yang, S., Paek, H., & Chen, M. The changing El Niño–Southern Oscillation and associated climate extremes. *Climate Extremes: Patterns and Mechanisms*, 1–38 (Wiley, 2017).
47. Li, X., Hu, Z. Z., McPhaden, M. J., Zhu, C. & Liu, Y. Triple-Dip La Niñas in 1998–2001 and 2020–2023: impact of mean state changes. *J. Geophys. Res. Atmos.* **128**, e2023JD038843 (2023).
48. Hasan, N. A., Chikamoto, Y. & McPhaden, M. J. The influence of tropical basin interactions on the 2020–2022 double-dip La Niña. *Front. Clim.* **4**, 1001174 (2022).
49. Yu, J. Y., Kao, H. Y. & Lee, T. Subtropics-related interannual sea surface temperature variability in the central equatorial Pacific. *J. Clim.* **23**, 2869–2884 (2010).
50. Di Lorenzo, E. et al. Central Pacific El Niño and decadal climate change in the North Pacific Ocean. *Nat. Geosci.* **3**, 762–765 (2010).
51. Iwakiri, T. et al. Triple-Dip La Niña in 2020–23: North Pacific atmosphere drives 2nd year La Niña. *Geophys. Res. Lett.* **50**, e2023GL105763 (2023).
52. Huang, B. et al. NOAA extended reconstructed sea surface temperature (ERSST), version 5. *NOAA Natl. Cent. Environ. Inf.* **30**, 25 (2017).
53. Kanamitsu, M. et al. Ncep–doe amip-ii reanalysis (r-2). *Bull. Am. Meteorol. Soc.* **83**, 1631–1644 (2002).
54. Lee, H. T., Gruber, A., Ellingson, R. G. & Laszlo, I. Development of the HIRS outgoing longwave radiation climate dataset. *J. Atmos. Ocean. Technol.* **24**, 2029–2047 (2007).
55. Behringer, D. W. The Global Ocean Data Assimilation System (GODAS) at NCEP. In *Proceedings of the 11th Symposium on Integrated Observing and Assimilation Systems for Atmosphere, Oceans, and Land Surface*. pp 14–18 (San Antonio, TX, Amer. Meteor. Soc., 2007).
56. Bretherton, C. S., Smith, C. & Wallace, J. M. An intercomparison of methods for finding coupled patterns in climate data. *J. Clim.* **5**, 541–560 (1992).

Acknowledgements

The research was carried out at the Jet Propulsion Laboratory, California Institute of Technology, under a contract with the National Aeronautics and Space Administration (NASA) (80NM0018D0004). The first author, J.-W.K., was supported by the NASA Postdoctoral Program fellowship administered by the Oak Ridge Associated Universities (ORAU) under a contract with NASA. The second author, B.T., was supported by the NASA Precipitation Measurement Mission Science Team (PMMST) program administered by Dr. Will McCarthy. The third author, J.-Y.Y., was supported by the NSF's Climate and Large-Scale Dynamics Program grant AGS-2109539. © 2024. All rights reserved. We acknowledge Dr. Yong-Fu Lin from Research Center for Environmental Changes for his assistance with pre-processing thermocline data from observations. We also express our gratitude to the providers of observational data and climate indices, whose contributions have made this study possible.

Author contributions

J.-W.K. and J.-Y.Y. designed the study. J.-W.K. performed the analysis, generated the figures, and wrote the initial manuscript. J.-W.K., B.T., and J.-Y.Y. contributed to interpreting the results and revising the manuscript.

Competing interests

The authors declare no competing interests.

Additional information

Supplementary information The online version contains supplementary material available at https://doi.org/10.1038/s41612-024-00890-0.

Correspondence and requests for materials should be addressed to Ji-Won Kim or Jin-Yi Yu.

Reprints and permissions information is available at http://www.nature.com/reprints

Publisher's note Springer Nature remains neutral with regard to jurisdictional claims in published maps and institutional affiliations.

Open Access This article is licensed under a Creative Commons Attribution-NonCommercial-NoDerivatives 4.0 International License, which permits any non-commercial use, sharing, distribution and reproduction in any medium or format, as long as you give appropriate credit to the original author(s) and the source, provide a link to the Creative Commons licence, and indicate if you modified the licensed material. You do not have permission under this licence to share adapted material derived from this article or parts of it. The images or other third party material in this article are included in the article's Creative Commons licence, unless indicated otherwise in a credit line to the material. If material is not included in the article's Creative Commons licence and your intended use is not permitted by statutory regulation or exceeds the permitted use, you will need to obtain permission directly from the copyright holder. To view a copy of this licence, visit http://creativecommons.org/licenses/by-nc-nd/4.0/.

© The Author(s) 2025